Contract No:

This document was prepared in conjunction with work accomplished under Contract No. DE-AC09-08SR22470 with the U.S. Department of Energy (DOE) Office of Environmental Management (EM).

Disclaimer:

Evaluation of Radiolytic Hydrogen Generation in the High Burnup Demonstration Dry Storage Cask - 21279

Anna L. d'Entremont*, Robert L. Sindelar*, Christopher G. Verst*, Ronald L. Kesterson*, Charles Bryan**, Brady Hanson***
*Savannah River National Laboratory, Aiken, SC
**Sandia National Laboratories, Albuquerque, NM
***Pacific Northwest National Laboratory, Richland, WA

ABSTRACT

Residual water (post-drying and sealing) in a spent nuclear fuel (SNF) dry storage canister/cask could include:

- free water trapped as a liquid and/or water as a vapor;
- physisorbed/chemisorbed water that is bound to internal surfaces, such as the cask and internals including fuel rods and aluminum components. This water is bound with varying adsorption energy, typically with the first few monolayers strongly bound with weakly bound layers forming on top in equilibrium with the humidity; and
- chemisorbed water that is chemically bound in an (oxy)hydroxide film.

These waters are subject to radiolysis from the attendant radiation of the fuel. The free and physisorbed waters radiolytically break down into molecular hydrogen and hydrogen peroxide, an oxidizing species, that itself would decompose into hydrogen and oxygen, with the oxygen expected to react with zirconium fuel cladding, resulting in net generation of hydrogen gas and ZrO_2. Radiolytic breakdown of chemically-bound water in (oxy)hydroxides can also occur to generate hydrogen gas.

The sources and amounts of residual water and the radiolysis thereof to cause hydrogen generation has been estimated for the High Burnup Demonstration (HBU Demo) Cask, a TN-32 cask loaded with high-burnup Light Water Reactor spent fuel assemblies and vacuum-dried at the North Anna Power Station in November 2017. The cask internals include 32 assemblies, each with 264 fuel rods clad in zirconium alloys, aluminum neutron absorber components, and aluminum and stainless-steel structural components. Empirical information from the literature for the radiolytic hydrogen yield in terms of G-values[a] has been applied to estimate the net H_2 expected from the separate radiolytic generation of the residual water inventories. Back-reactions in the helium cover gas are not expected, and gettering of H_2 was assumed to be negligible due to material condition of a hydride rim (hydrogen-saturated condition) on the HBU fuel cladding surface.

The results for the estimation in terms of H_2 concentration in the cask volume in ppmv at two points in time are shown in the table below. For the 12-day time, two cases were considered: 1) case 1 assumes that the physisorbed/chemisorbed water present on the cladding surface following dry-out is not replenished by water vapor in the cask; 2) case 2 assumes that water vapor in the cask quickly replenishes the cladding surface water due to high affinity to the ZrO_2 on its surface.

The radiolytic hydrogen generated at 12 days duration was estimated at 534 ppmv for Case 1, in good agreement to the ~500 ppmv measured from a gas sample from the HBU cask. This paper describes the bases for residual water and hydrogen estimation in the HBU Demo cask. The application of the results shows there are no canister pressurization or flammability issues with extended dry storage of SNF.

[a] The G-value is typically given in units of molecules of H_2 per 100 eV or in units of μmol of H_2 per Joule for energy deposited into the water-bearing material component. 1 μmol/joule = 9.63 molecules/100 eV

Estimation of hydrogen production due to water radiolysis in the HBU Demonstration Cask

H_2 Source	Total H_2 inventory (ppmv)	H_2 production in 12 days (ppmv)				H_2 production in 40 years (ppmv)
		Assuming no H_2O replenishment of surface water (Case 1)		Assuming rapid H_2O replenishment of surface water from water vapor (Case 2)		Assuming H_2O replenishment
Free/surface water	20554	0.01	(steel)	0.01	(steel)	20554
		520.3	(ZrO_2)	16133	(ZrO_2)	
		8.7	(vapor)	8.7	(vapor)	
Chemisorbed water (bayerite on aluminum rails)	86946	4.67		4.67		3711
Total H_2	107500	534		16146		24265

Notes: 1) The radiolytic hydrogen gas generation rates ("G-values") were taken from the literature for the estimation. A single constant dose rate (energy deposition rate) of 3×10^{15} eV/g/s was used to calculate the 12-day values of radiolytic hydrogen generation. The 40-year values were estimated using the average dose rate of (0.653)(3×10^{15} eV/g/s) to account for exponential decay with the half-life of Cs-137 (30.05 y), starting from 3×10^{15} eV/g/s. 2) The fuel rod surfaces are assumed with an attendant layer of ZrO_2 oxide and crud on which initial physisorbed/chemisorbed, and pore waters are estimated. 3) The aluminum surfaces are assumed with a bounding thick attendant layer of hydrated oxide. 4) Chemical back reactions, and gettering by zirconium, that would reduce the H_2 level in the cask are neglected.

INTRODUCTION

In any enclosure with materials (e.g. canister with fuel and canister internal structures), drying can leave an inventory of residual water [ASTM C1553-16]. This paper estimates the water sources present in the High Burnup Demo storage cask from North Anna [Bryan et al, 2019a] and the radiolytic H_2 generated therefrom. Figure 1 is a top view of the cask prior to loading. After the fuel assembly loading into the demo cask and in preparation for long-term storage, water was drained from the cask and numerous blowdowns were done to further enhance the water removal. The drying process involved a sequence of vacuum and hold conditions with the cask (internals) brought to an initial 55 Pa (0.41 Torr) vacuum with pressure being allowed to rise for about eight hours, followed by a backfill with helium to a pressure of 32 psi (2.2×10^5 Pa) [Bryan et al, 2019a]. The cask contains 32 spent fuel assemblies.

The loading of SNF into dry storage casks and the subsequent drying operation can leave small amounts of residual water in the sealed casks. This water could be in the form of:

a) Liquid water at the cask bottom or in isolated areas in the fuel assembly and cask internal structures. (This would be inadvertent free water that could only be from trapped water or frozen water at a local cold spot.)

b) Water vapor as humidity in the cask internal environment. (At a 3 torr pressure, approximately 0.43 moles of free water in the form of water vapor is assumed to remain in the canister [Knoll, 1987].)

c) Physisorbed/chemisorbed water on component surfaces including water retained strongly by capillary forces in pores and fissures in the crud and fuel rod oxide. (A partitioning of the free water between water vapor and monolayers of water on the surfaces will occur.)

d) Chemisorbed water in hydrated oxides and crud films. (This refers to water that is chemically bound as hydrated oxides.)

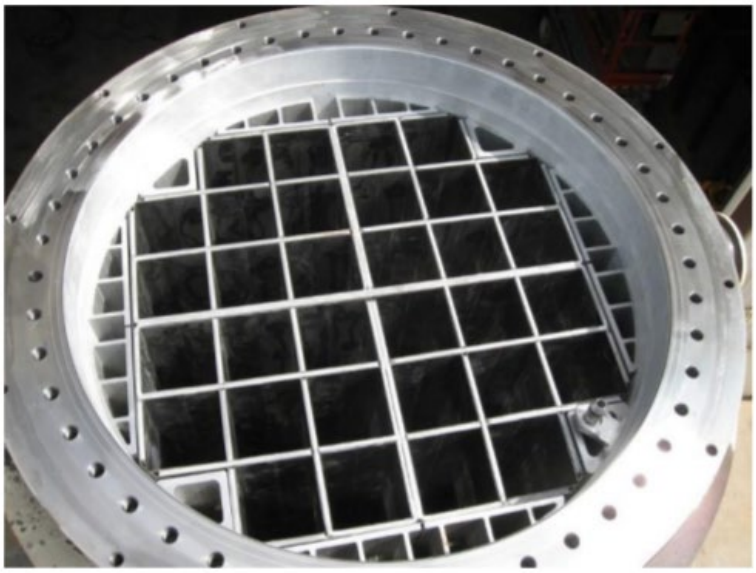

Figure 1. Top view of Demo cask internals [Hering, 2016]. The photo, courtesy of AREVA TN shows cask that EPRI equipped with special instruments to measure the behavior of high burnup fuel

Residual water (post-drying and sealing) in a spent nuclear fuel (SNF) canister can result in corrosion and radiolysis that can affect the spent nuclear fuel and canister internal structural materials [CNWRA 2013, Shukla et al, 2019, ASTM C1553-16].

Radiolytic breakdown of free water with gamma radiation occurs readily with waters on surfaces of a substrate vis-à-vis radiolytic breakdown of water as a vapor due to energy deposited into the substrate that is assumed to contribute to the radiolytic process. The residual water inventory also includes water in hydrated oxides that is also termed "chemisorbed" water. H_2 release only (i.e., no observed oxygen release) has been reported from radiolysis of chemisorbed water. Hydrogen yields from radiolysis of waters of material systems are determined empirically.

An important phenomenon is the radiolysis of the residual free water creating H_2 and H_2O_2, an oxidizing species that is expected to quickly break down on surfaces and cause oxidation reactions with the cladding, exposed fuel, and other materials in the canister. With radiolysis of the residual free water, and consumption of oxygen, H_2 would be the net product in the canister free volume. The observations from the work in 2019 [Shukla et al, 2019] showed that radiolytic breakdown while the fuel was relatively hot (compared to its cooler temperatures following years of post-discharge cool-down) would result in a higher oxidation rate of any "hot" exposed fuel (UO_2)[b] relative to the oxidation of the cladding. In contrast, oxidation at low fuel/cladding temperatures (< ~300°C) would occur primarily with the cladding and non-fuel materials in

[b] Exposed fuel is highly unlikely as it requires a breach in fuel cladding.

a canister that contains exposed fuel. Thus, characterization of the rate of radiolysis is important to refine the estimation of impacts of residual water.

Hydrogen gas is the expected net gaseous product of radiolytic breakdown of water due to the mechanisms described above. Bryan [Bryan et al, 2019a] observed H_2 at ~500 ppmv after 12 days post dry-out of the High Burnup (HBU) Demonstration Cask. A rigorous comparison of that result to an estimate of radiolytic hydrogen production had not been made.

This present work supplements the evaluation of water sources in SNF canisters [Bryan et al., 2019b] and uses the specific materials and the configuration of the HBU cask to estimate the residual water content from all sources at the time of initial sealing.

This present paper estimates the hydrogen generation via radiolytic breakdown of the waters in the HBU cask, and the paper draws information extensively from a topical report [d'Entremont, et al, 2020]. Hydrogen content is a measure of the extent of radiolysis that has occurred in the canister and an indirect indicator of the residual water in a canister. It is recognized that the generation of hydrogen from radiolysis in an SNF canister does not pose a flammability concern if the oxygen concentration remains sufficiently low, as is expected based on current data [Sindelar, et al, 2020].

The predicted radiolytic yield is sensitive to the accuracy of both the initial water inventory estimates and to the assumed radiolysis behavior associated with different regions/surfaces in the canister. The radiolytic yield produced at a given location in the cask (e.g., a component surface) is limited by the total amount of residual water available to be broken down at that location, which is determined by the assumptions regarding the initial residual water inventories and also how the various free and surface water inventories interact. In general, when a dry oxide surface is exposed to humid air, first hydroxyl groups and then some number of layers of molecular water form on the surface, depending on the relative humidity, until the surface water and water vapor are in equilibrium. If either the water vapor or surface water is depleted by a mechanism such as radiolysis, then it is expected that water will adsorb/desorb to the surface to reestablish equilibrium. The assumption of whether or not this mechanism replenishes surface water during radiolysis in the cask has major impact on the radiolysis predictions.

CASK GEOMETRY

The HBU Demo cask has inner dimensions of 163.250" (4.14655 m) tall and 68.750" (1.7463 m) diameter [Jenson, Drawing of TN-32 cask, Waldrop, 2020], yielding a total cask volume of 9.9309 m^3. The nominal free volume in the cask is estimated to be about 5.96 m^3 assuming a 60% internal free volume.

The same internal dimensions yield a nominal surface area for the uncoated steel liner of 27.538 m^2 (22.748 m^2 for the sides plus 4.7900 m^2 for the ends). Assuming only one side of the liner is exposed to the interior environment, 27.538 m^2 is the total surface area associated with the cask interior.

Figure 2 is a schematic of the cell matrix structure used for thermal modeling and shows the structural material layout in cross-section (not to scale). The cell matrix has 32 cells to hold fuel assemblies, each 8.700" (22.098 cm) square from wall to wall [Jenson, Drawing of TN-32 cask from Waldrop, 2020]. The walls between cells are constructed of layered plates. Per Fort [Fort et al, 2019], "the basket cells are formed […] with stainless-steel sheets on the outer faces of the basket structure. Much thicker aluminum alloy plates are sandwiched between the stainless-steel plates, with double-thickness aluminum plates forming the central 'cross' of the basket." According to the schematic for thermal modeling [Jenson, Drawing of TN-32 cask], the center "cross" cell walls are 1.080" thick (including both aluminum and steel), and the narrower cell walls are 0.540"-thick aluminum sandwiched between 0.105"-thick stainless-steel plates.

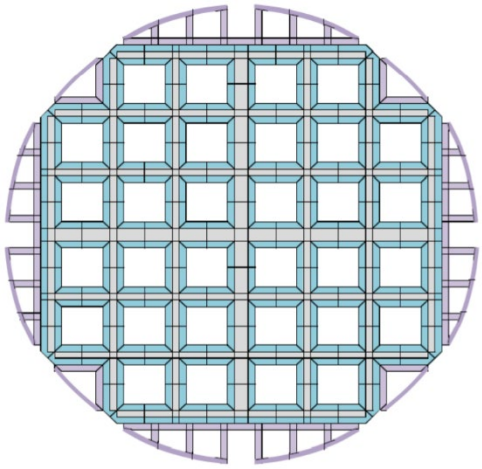

Figure 1 Diagram of 3-D COBRA-SFS model of TN-32B basket – aluminum rails in purple, stainless steel fuel compartments in blue, and structural aluminum structures in grey (Note: diagram not to scale; thicknesses greatly exaggerated for clarity) [Fort, 2019]

The interior surface area of a single cell is given by $4(8.700\text{ in})(160.000\text{ in}) = 5568\text{ in}^2 = 3.592\text{ m}^2$. The total cell surface area for all 32 cells is 115.0 m^2. (This is the exposed area associated with the stainless-steel cell liners.)

Details of the cask design are not readily available, and it is not certain how much of the interior aluminum plates in the cell matrix would be exposed for (oxy)hydroxide formation and potentially contribute to radiolysis. The current analysis assumes that the faces of the aluminum structural plates and neutron absorbers are protected from exposure by the stainless steel plates, and that the exposed end area of the plates is negligibly small compared to the other surfaces in the canister. Therefore, the aluminum in the cell matrix is not included in the base aluminum surface calculation.

Rails

The supporting rails positioned between the straight sides of the basket cell matrix and the curved cask cylinder are aluminum and comprise a significant surface area of exposed aluminum. The surface area of the rails is more complicated to calculate than that of the basket cells, but as a first approximation, the rail plates have a total estimated exposed surface area of 86.29 m^2 [d'Entremont, et al, 2020].

Fuel Rods and Additional Zr Components

Bryan [Bryan et al, 2019b] gives the surface area of a single PWR fuel rod as 0.115769 m^2. Each assembly contains 264 fuel rods [Bryan et al, 2019b], and the HBU Demo cask contains 32 such assemblies. This yields a total fuel rod surface area of 978 m^2 for all rods in the cask.

Additional zirconium alloy components also exist in the fuel assemblies [Bryan et al, 2019b]. The additional area of these components is approximated here as about 37% of the fuel rod surface area.

Helium Backfill

The cask pressure is 2.2 bar, and the free volume is 5.96 m^3. Using an estimated average temperature of 135°C and the ideal gas law, this yields an estimated 386 mol He in the cask backfill.

WATER SOURCE POST DRY-OUT

Liquid Water

Bryan [Bryan et al. 2019a] reports that, assuming a homogeneous gas phase in the cask, the humidity levels in the gas samples indicate no free liquid water, only water vapor, remaining in the cask unless liquid water had been trapped in occluded locations. At assembly loading in the pool, there is a probability that some of the thimble tubes could contain water but only if the drain hole was plugged by debris settling during storage. As discussed by Bryan [Bryan et al, 2019a,b], it is expected that the cask high-temperature drying will evaporate any water retained at loading. Thus, a thimble tube water source is not included in this evaluation.

There is a potential for boric acid H_3BO_3 precipitation from PWR spent fuel pool (SFP) to be in the canister as discussed by Bryan et al [Bryan et al, 2019b]. At a nominal SFP concentration of 2000 ppm of boric acid, there would be 0.2 moles of boric acid per liter of pool water that evaporates in a canister. At a temperature of 150°C, full dehydration of 0.2 moles of H_3BO_3 would produce 0.3 moles (6 grams) of water together with boron oxide, B_2O_3. Due to high uncertainties of the amount of residual water following blowdown that would remain in the canister, and the amount, if any, of H_3BO_3 that did not thermally decompose during the drying process, this potential water source is not included in this evaluation.

Thicker oxides (typically >50 microns), if present on the fuel rods, will have some degree of fissuring or incipient delamination due to the stresses generated in the oxide during formation. These fissures will act as pores to retain some water from operation and storage in the fuel pool. Upon drying for cask storage, it is postulated that the majority, if not all, of this water source will be converted to steam during the drying process and removed.

Liquid water evaluation is excluded from this study. Free water is considered to be in vapor form only.

Water Vapor

Bryan [Bryan et al, 2019a] reported the presence of water vapor in the sampled cask gas at a level of 17,400 ppmv at 65°C. With uncertainties, a 2% (20000 ppmv) value for initial water vapor in the cask internal gas is included in the current analysis.

Physisorbed/Chemisorbed Water on Component Surfaces

The stored fuel and adjacent structures are relatively hot as shown in the temperature models, Figure 3, from [Fort, 2019]. Surface-adsorbed water can have varying adsorption energies, often with the first few monolayers strongly bound to the surface and additional, more weakly bound layers forming on top due to equilibrium with the humidity. Weakly physisorbed water is assumed to be present only on the cooler surfaces of the cask wall (i.e., on the steel liner) and assumed to be absent on the fuel surfaces due to the temperature and the drying procedures. The mass of a single-molecule-thick physisorbed water layer is reported to be between 0.187 and 0.3 mg/m^2 [Petrik, 2001; Wertsching, 2007]. A value of 0.3 mg/m^2 is used in this evaluation.

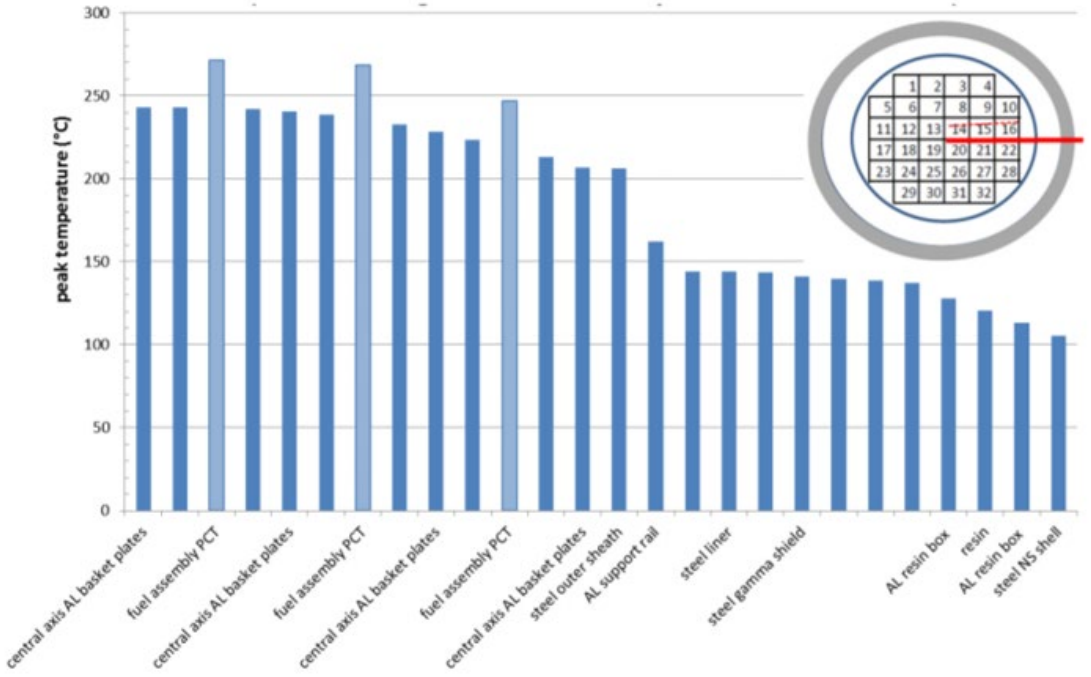

Figure 3. Radial distribution of system component temperatures at the axial location of Peak Cladding Temperature for initial storage conditions (as of 7/31/2017) [Fort, 2009]

In this study, "chemisorbed water" is strictly defined as the water that is incorporated chemically in hydrated oxides such as aluminum (oxy)hydroxides. This water can be present in the cask and associated hydrated surface oxides on the structural steel, fuel assembly components (primarily fuel rod oxides and crud), and in oxides on aluminum structures and neutron absorber plates (borated aluminum panels).

Stainless Steel

Per Dylla [Dylla, 2006], the strongly bonded physisorbed/chemisorbed water on stainless steel is less than a monolayer in thickness on an actual surface area basis, but is equivalent to about five monolayers when considering effective geometric surface area. Additional layers of physisorbed water are weakly bound and reported to easily desorb in vacuum and are thus expected to be absent everywhere but near the outer perimeter of the cask with the lowest temperatures.

As previously estimated, the nominal exposed stainless-steel surface area is about 27.5 m^2 for the cask liner plus 115.0 m^2 for the cell matrix for a total of 142.5 m^2, plus we add 10% for effective surface area. It is conservatively assumed that there are five monolayers of strongly physisorbed/chemisorbed water on the steel surface. In addition, 25% of the cask inner surface is assumed to have one layer of weakly physisorbed water (conservative, since at the cask humidity there is typically less than a monolayer coverage predicted).

The strongly physisorbed/chemisorbed water inventory for the steel components is calculated by multiplying the total effective surface area by the chemisorbed water loading, i.e., $1.1(142.5\ m^2)(5\ \text{monolayers})(0.3\ \text{mg}/m^2/\text{monolayer}) = 235.1$ mg or 0.01306 mol H_2O. If all of this H_2O produced molecular H_2 under irradiation, then dividing 0.01306 mol H_2 by the estimated 386 mol He estimates 33.8 ppmv H_2 contributed by water strongly physisorbed/chemisorbed on steel. A similar calculation for 0.25 monolayers of weakly physisorbed water on only the cask liner area yields 2.272 mg / 1.26×10^{-4} mol H_2O, contributing a maximum of 0.327 ppmv H_2.

Fuel Assembly

There are two potential sources for retained water in the fuel rod surface oxide. One is molecular water films physisorbed/chemisorbed on the surface, and the other is retained water in the oxide fissures. Typically, oxides over about 40 μm in thickness contain fissures in the structure that can contain residual water. It is expected that some of this water will be vaporized and escape during the heated drying operation.

Many investigators [Agayev, 2017; Skotnicki, 2015; Petrik, 2001; Holmes, 1974; Köck, 2016; for example] have evaluated the strong physisorption/chemisorption of water on ZrO_2 using powders, thin lab-grown oxides, and some with added solutions for scavenging radiolysis species. It is reported that hydroxyls are formed at the oxide surface when water is present, and these hydroxyls act as anchors for one or a few molecular layers of adsorbed water. It should be emphasized that this is a surface effect that does not involve chemically incorporated water throughout the bulk of the oxide, unlike the chemisorbed water associated with aluminum alloys. Thus, the adsorbed water source is relatively limited even with the large rod surface area. Bryan [Bryan et al., 2019b] estimates the physisorbed/chemisorbed water on the fuel rod oxide surface to be about 12 mg per assembly. In this evaluation, we find a value of about 10 mg of physisorbed/chemisorbed water per assembly with a single water layer. However, for the base calculations, we include 3 water layers. Information on oxide fissures and flaking is qualitative and varies from rod to rod, making it difficult to estimate the water contribution. For this sensitivity evaluation, oxide fissures are assumed to contribute a water/hydrogen quantity equal to the nominal surface water. The rate of water removal with cask drying procedures is not known, although it is speculated that some physisorbed/chemisorbed water will be removed with drying. The contribution to the radiolytic H_2 generation from fuel rod surfaces is included in the hydrogen generation evaluations.

Crud is observed on some fuel rods. For PWR rods, the crud is generally black or shades of gray and consists of partially substituted nickel ferrite or spinel with (generalized) composition $Ni_xFe_{3-x}O_4$ (with x ranging from 0 to 1) [Hazelton, 1987]. Reference [Hazelton, 1987] provides a good historical crud review. Some crud contains oxyborates that have been associated with an axial offset anomaly. The presence of crud on fuel rods varies greatly between plants, between assemblies, between rods in assemblies, and axially along fuel rods. There are two general types of crud: flocculant (loosely adhering) and tenacious (denser and more strongly adherent). When present, the crud is observed at the hottest rod locations and typically not over the full rod length.

Crud consists of anhydrous compounds and is considered for this evaluation to not include chemisorbed water, although there is probably some small amount of molecular-thin chemisorbed water film on the particles. The bulk of the water source associated with crud is related to the porosity and is included in the physisorbed / pore water.

The crud can have >50% porosity. Unlike the aluminum (oxy)hydroxides, the crud is anhydrous, so the main potential for retained water is associated with the crud porosity. It is postulated that the majority of the water entrained in the crud will be removed by the dry gas purge and the vacuum evaporation and that the crud temperature will be similar to the fuel rod temperature, precluding water re-condensing. One approach to estimate the equivalent water retained in the crud is to assume that the free water was removed during drying and the porosity in the hot crud is now in equilibrium with the water vapor in the cask. With this assumption, it can be concluded that the water vapor in the crud does not have a significant impact on the total water inventory in the cask. For this sensitivity evaluation, it is assumed that the crud effectively doubles the rod surface area and contributes an amount of hydrogen equivalent to the nominal ZrO_2 physisorbed/chemisorbed source.

The total nominal area of all fuel rods was estimated to be 978 m^2. Adding the 37% surface area for additional Zr components gives a total ZrO_2 surface area of 1340 m^2. Accounting for three monolayers of water at 0.3 mg/m^2/monolayer and multiplying by a factor of three to account for the oxide fissures and crud, the total mass of water is estimated as 3.62 g or 0.201 mol H_2O (0.147 mol on the fuel rods and 0.0543

mol on the additional Zr components). Dividing 0.201 mol H_2 by the 386 mol He estimates the maximum H_2 yield from physisorbed/chemisorbed water on ZrO_2 as 520.3 ppmv.

Aluminum Alloys

Unlike the steel and zirconium alloy components, which only have molecular-scale surface water films, aluminum can form (oxy)hydroxide or "hydrated oxide" films containing bonded hydrogen and oxygen in 2-to-1 ratio, i.e., chemisorbed water throughout the oxide. Radiolysis occurring due to the radiation field within the cask will interact with the oxide, and, through radiolysis, hydrogen will be generated.

The exposed aluminum surfaces may have hydrated oxide (aluminum (oxy)hydroxide) formed from ambient exposure and potentially additional oxide formed during the initial stages of high-temperature drying if sufficient water vapor is present. At low temperatures, primarily trihydroxides ($Al(OH)_3$ or $Al_2O_3 \cdot 3H_2O$), i.e., gibbsite or bayerite, would form, but depending on the thermal exposure during drying, the gibbsite may thermally decompose to boehmite (AlOOH or $Al_2O_3 \cdot H_2O$). Based on the molecular weights, about 34.6% ($M_{3(H2O)}/M_{Al2O3 \cdot 3(H2O)}$=54/156) of the bayerite/gibbsite mass is water and 15.0% ($M_{H2O}/M_{Al2O3 \cdot H2O}$=18/120) of the boehmite mass is water. The surface (oxy)hydroxides contain chemisorbed water that is not expected to be totally removed during the cask drying and is considered a source for H_2 from radiolysis during storage. Bayerite films approximately 8 μm thick have been observed on aluminum after 36 days immersion in room-temperature liquid water [d'Entremont, 2020b]. This analysis will assume 8 μm of bayerite as a starting point, which is expected to be conservative since the rails are not expected to have a significant history of immersion in water other than the cask loading process. If thermally decomposed to boehmite during drying, the 8 μm of bayerite would result in ~5.2 μm of boehmite, assuming negligible spalling. To evaluate the total water inventory in the film, the (oxy)hydroxide density of 2.53 g/cm^3 is used for bayerite and 3.01 g/cm^3 is used for boehmite [Wefers, 1987].

Assuming 8 μm thick film of bayerite remaining as bayerite after drying, the mass of oxide is about 1750 g, containing 605 g or 33.6 mol H_2O. Dividing 33.6 mol H_2 by the estimated 386 mol He yields 8.69% or 8.69×10^4 ppmv from bayerite.

Radiolysis of water sources and hydrogen generation

The focus of this section is to evaluate the potential hydrogen generation with radiolysis of the water sources in the cask after drying and closure. Gettering of hydrogen by reactions with the fuel clad and other zirconium alloys is not included. Chemical back reactions were neglected.

G_{H2} Values

G_{H2} represents the production rate of hydrogen molecules during radiolysis of hydrogen-containing materials. G_{H2} values vary greatly depending on the material being irradiated, the environmental parameters, and the radiation characteristics.

The gamma radiolysis of H_2O has been studied extensively. The radiolysis results in the rapid formation of molecules, atoms, ions, and radicals. These products react and form stable components (H_2, H_2O_2, and H_2O). The rates of production by radiolysis are designated by the G-value, which is reported in units of molecules, ions, or radicals (depending on the product) per radiation dose. For H_2, G_{H2} is reported in molecules of H_2 per 100 eV or in μmol H_2 per joule (1 μmol/joule = 9.63 molecules/100 eV). The relative quantities of the stable components and the resulting calculated G are dependent on the characteristics of the system/environment in which they are being produced and are not constant values across differing systems.

The factors that affect G-values have different impacts depending on the species being measured. A focus of this evaluation is to examine the production of hydrogen inside the demo storage container for spent nuclear fuel (SNF); thus, the discussion of G-values will be directed mainly to the impact on H_2 production.

Temperature

Elliot [Elliot, 2009] summarized data regarding the effect of temperature on G_{H2} from several literature sources. The summary is shown in Figure 4 and indicates an increasing G_{H2} with temperature. Some of the data points were generated in water with added solutions which can impact the G value by scavenging and reacting with other species from the radiolysis. The trend line follows the data that was extrapolated to zero concentration and is consistent with the typical G_{H2} value from Spinks of 0.45 molecules/100 eV. The trend line follows equation {1} and has a G_{H2} value of 0.44 molecules/100 eV at 23°C and 0.56 molecules/100 eV at 250°C for the system that was used to determine the values. The temperatures within the fuel element storage cask vary and will decrease over time but the G_{H2} value in the cask is expected to have relatively small temperature-related variation and is expected to remain below 0.6 molecules/100 eV for the storage conditions.

$$G_{H2} = 0.419 + 8.721\times10^{-4}\,T - 4.971\times10^{-6}\,T^2 + 1.503\times10^{-8}\,T^3 \qquad \{1\}$$

where T is the temperature in °C and G_{H2} is given in molecules/100 eV.

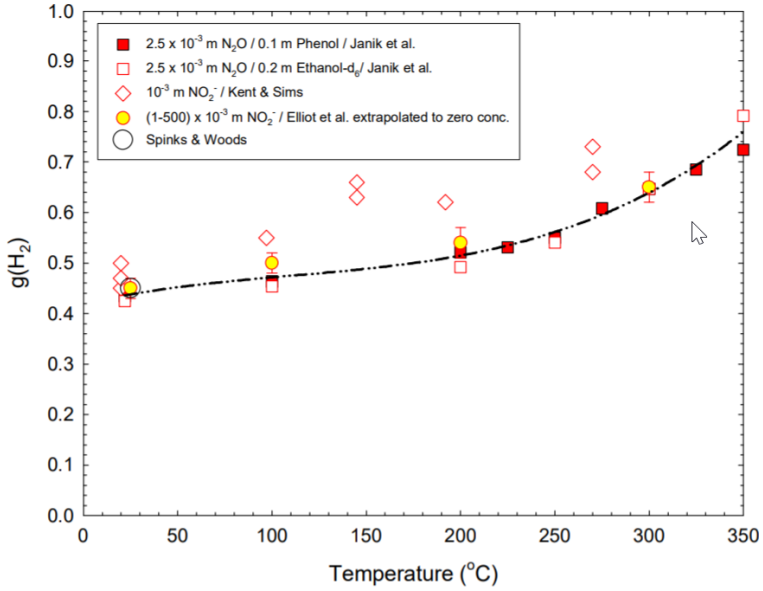

Figure 4 Temperature Effect on G_{H2} [Elliot, 2009]

System Environment

The system environment, cover gas or liquid solutions, will affect the amount of free hydrogen generated in the system and also the calculated G-value. The presence of scavenger species can affect the hydrogen production by interfering with precursor radicals produced in the radiolysis. For the evaluation of hydrogen generation in the SNF cask, the environment is relatively pure with only helium cover gas, so there should be no significant impact on the G_{H2} values due to chemical reactions with the cask gas environment (except for possible minor effects from small amounts of residual air and hydrocarbons). However, the environmental impacts on reported G_{H2} values in the literature need to be evaluated to assess their applicability to applications where pure water or water vapor are being considered since the G-value is system environment dependent.

Alloy Surface and Substrate

Elliott [Elliott, 2009], discussing radiolysis of physisorbed and chemisorbed water, reported that the substrate where the water is adsorbed or retained as radicals has an impact on the hydrogen production rate and corresponding G-values. Westbrook [Westbrook et al, 2015] reported that two different aluminum (oxy)hydroxides, boehmite and gibbsite, produce hydrogen at different rates under gamma radiation. La Verne [La Verne, 2009] reports different hydrogen production rates for powdered oxides of U, Zr, and Ce. For the evaluation of radiolysis in storage casks, the primary surfaces are the zirconium-alloy fuel rods with an oxide surface that was grown during operation, steel structural components, and aluminum structural rails.

When evaluating representative G-values, the substrate morphology also needs to be considered. For example, a significant portion of the G studies reported in the literature are based on using oxide powders, powder-compacted pellets, or thin lab-grown oxides. The powder/thin oxide structure, porosity, and surface area can differ widely from the morphology of operationally grown oxides on base metal surfaces and lacks applicable SNF metal-substrate-related effects.

There have been numerous reports on radiolysis of water in contact with ZrO_2 powders and crystals and evaluations of the effects of surface physisorbed/chemisorbed water. Garibov [Garibov et al., 2015] reports a G_{H2} value of 2.14 molecules/100 eV for adsorbed water on nano-ZrO_2 powder at a temperature of 300 K (with increasing G-value as the temperature increased). Petrik et al. [Petrik et al., 2001] also observed high G-values for water adsorbed on ZrO_2 powders compared to pure water. However, they also studied ZrO_2 doped with Nb^{+5} and with Li^+ or Rb^+, and for the ZrO_2 powders doped with Nb^{+5}, the hydrogen production was significantly reduced as shown in Figure 5 [Petrik et al., 2001]. Doping the ZrO_2 powders with Li^+ or Rb^+ increased the radiolytic H_2 yield by a factor of 2 at 0.1% mass of the dopant [Petrik et al., 2001], so the presence of dopants can either suppress or enhance H_2 production depending on the dopant. It was postulated that the defects in the oxide crystal lattice is an important factor impacting water radiolysis occurring on ZrO_2 surfaces. It is important to note that most, if not all, of the ZrO_2 radiolysis studies use very pure material: fine powders, crystals, or very thin lab-grown oxides with no Nb or other alloying elements present. Since the clad on the ZIRLO and M5 rods have 1% Nb as an alloying additive, the resulting oxide will also contain Nb along with other precipitates that produce lattice defects. While the two Zirc-4 assemblies do not have Nb in the cladding alloy, they do have Sn, Cr, and Fe which will also result in lattice defects. It is assumed that the 7% of rods in the cask will have similar radiolytic surface characteristics as the Nb containing rods. Based on these observations, the G_{H2} value used in this study for the fuel rod oxide is the value observed for typical water radiolysis of 0.47 molecules/100 eV, i.e., neglecting any potential enhancement due to the presence of the ZrO_2 surface or suppression due to the Nb content.

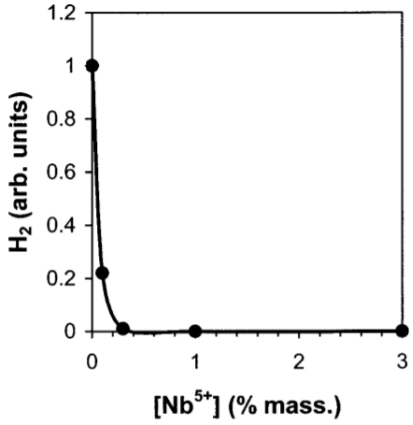

Figure 5. Effect of Nb^{+5} doping of ZrO_2 on the radiolytic H_2 production from adsorbed water [Petrik et al., 2001]

Kaddissy [Kaddissy, 2016] and Westbrook [Westbrook et al., 2015] both studied the radiolytic hydrogen production from gamma irradiation of hydrated aluminum oxides. G_{H2} results are summarized in Table 1 for $Al(OH)_3$ powders and for small and large AlOOH powders. The larger powder size is more analogous to the oxide films grown on aluminum surfaces, and G_{H2} reported for the larger boehmite powders ranged from 0.048 to 0.13 molecules/100 eV, i.e., roughly one tenth to one quarter of the typical reported G_{H2} for water. For this evaluation, G_{H2} values of 0.05 and 0.02 molecules/100 eV are used for the boehmite and bayerite calculations, respectively.

Table **1.** G_{H2} measured for various $Al(OH)_3$ and AlOOH powders from two studies. Values for "large" boehmite powder ranged from 0.048 to 0.13 molecules/100 eV [Kaddissy, 2016].

Material	**$G(H_2)$ (mol/J) $\times 10^{-8}$**	**$G(H_2)$ (molecules/100 eV)**	**Reference**
AlOOH (large)	0.57-1.3	0.055-0.13	[Westbrook, 2015]
AlOOH (large)	0.5 ± 0.2	0.048 ± 0.02	[Kaddissy, 2016]
$Al(OH)_3$	0.21 ± 0.05	0.020 ± 0.005	[Kaddissy, 2016]
AlOOH (small)	0.04 ± 0.02	0.004 ± 0.002	[Kaddissy, 2016]
$Al(OH)_3$	Low, not evaluated	Low, not evaluated	[Westbrook, 2015]

Gamma Dose and Initial Transition Effects

The long-term, steady-state G-values are critical data when evaluating water radiolysis in dry storage systems. The G-values calculated from initial irradiation doses can be/are different than the long-term doses when a quasi-steady-state condition evolves including back reactions and environmental effects. An example of this is shown in Figure 6 with measurements of Arkhipov [Arkhipov, 2007], where G-values were measured in water vapor for different accumulated doses and radiation dose rates. Initially, the calculated G_{H2} values are high—close to 9 molecules/100 eV, but as the dose accumulates over time, the G-value decreases. To obtain an estimate of the longer time/dose G-value, a set of representative points was obtained from the graph and are listed in Table 2. These data points are plotted in Figure 7 and indicate that the G-value is not affected by the range in dose rates, Gy/s, but is instead only a function of the total accumulated dose. The trend line for the curve was calculated to be $G_{H2} = (22.793 \text{ molecules kGy}^{0.568}/100 \text{ eV})(\text{dose})^{-0.568}$ and suggests an asymptotic approach to a steady state G-value. Extrapolating the fit to a dose of 1000 kGy predicts a value of $G_{H2} = 0.45$ molecules/100 eV. This value is in the same range as typically used for H_2 yield from water and emphases the risk of using low-dose G-values for longer-term (quasi-steady-state) calculations.

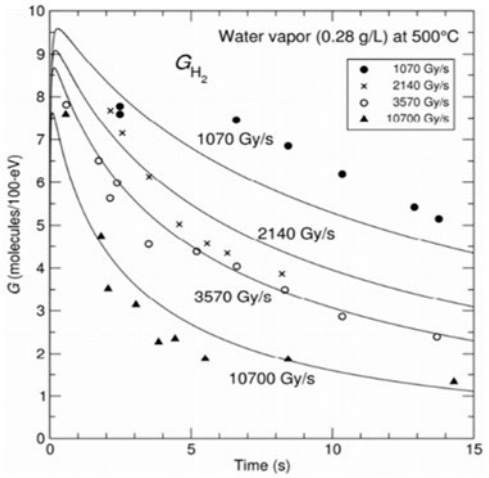

Figure 1. Hydrogen yield over time for water vapor for various radiation dose rates [Wittman, 2013]

In addition to the total dose/steady state influence on G, the radiation energy level can affect the measured G-value [Le Caër, 2011; Kabakchi et al., 2013; Wang, 2013]. Wang's [Wang, 2013] summary of G-values reported by researchers incorporating different radiation energies is shown in Table 3. Here, the value of G_{H2} ranged from 0.45 to 1.8 molecules/100 eV depending on the energy of the radiation. The lower-LET gamma ray energy is applicable to the current evaluation.

Table 2. Selected data points from Figure 6 for replotting

Gy/sec	Time seconds	kGy - total	G_{H2}
1070	14	15	5.1
1070	6.5	7	7.5
1070	8.5	9	7
3570	14	50	2.4
3570	7	25	4
3570	2.5	9	6
10700	14.5	155	1.4
10700	6.5	70	1.9
10700	4	43	2.5
10700	2	21	4
10700	1	11	6

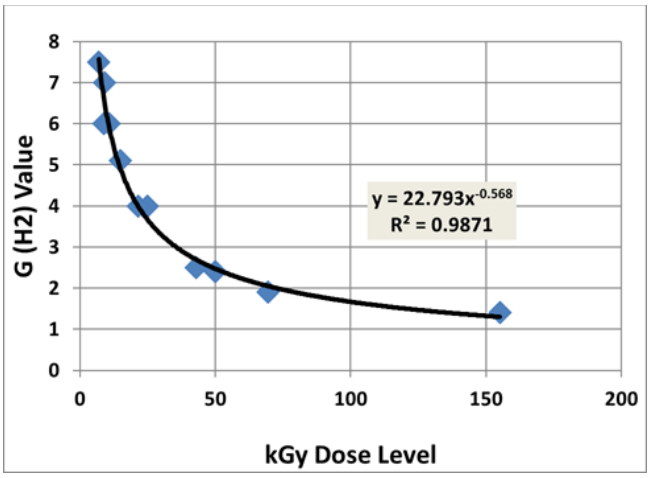

Figure 2. Data points from Figure 6/Table 2 for multiple dose rates plotted as a function of dose, with a power-law fit (G in units of molecules of H_2 per 100 eV energy deposited)

Table 3. Primary yields (in molecules/100 eV) of products of water radiolysis under different types of radiation at room temperature [Wang, 2013]

Source	LET (keV/μm)	g(-H_2O)	g(e^-_{aq})	g(OH)	g(H)	g(H_2)	g(H_2O_2)	g(HO_2)
^{60}Co γ-ray [39]	0.23	4.08	2.63	2.72	0.55	0.45	0.68	0.008
H^+ [39]	12.3	3.46	1.48	1.78	0.62	0.68	0.84	-
Fast neutron [40]	40	3.19	0.93	1.09	0.50	0.88	0.99	0.04
He^{2+} [39]	108	2.84	0.54	0.54	0.27	1.11	1.08	0.07
^{10}B(N, α)^{7}Li [41–43]	220	3.9	0.33	0.30	0.10	1.8	1.67	0.13

Radiolysis in Water Films Versus Water Vapor

For the evaluation of water radiolysis in the SNF cask, two types of water are assumed to be present, water that may be present as surface adsorbed films and water vapor in the cask environment associated with humidity levels. Yousefi [Yousefi, 2014] reports results from two sources comparing G_{H2} values in liquid water and water vapor. The comparison is shown in Table 4, first in the reported units of micromoles per joule and then converted to molecules/100 eV (1 µmol/J = 9.63 molecules/100 eV). The values were obtained from [Elliott, 2009] and [Arkhipov, 2007]. There is a significant difference in the G-value of most species for liquid versus vapor, but the G_{H2} value is similar for both, with the vapor value being slightly higher. Other reported values for G_{H2} for steam and water vapor vary from 0.05 [Boyd, 1973] to >2 (beta radiation at elevated temperature) [Boyd, 1963]. G_{H2} for pure liquid water is reported by [Crumière, 2013] as 0.25-0.30 molecules/100 eV as compared to a typical value of 0.46 molecules/100 eV in a system where a substrate is present on which the water can be physisorbed or chemisorbed. Liquid water is assumed not to be present in the cask, so a G_{H2} for liquid water will not be used. The value for water vapor based on [Arkhipov, 2007] of 0.47 molecules/100 eV will be used for the comparative calculations.

Table 4. Primary yields of water radiolysis under γ irradiation 25°C [Youssefi, 2014], as originally reported in μmol/J and converted to molecules/100 eV

Water phase	G units	H_2O	$\cdot e_{aq}^-$	H^+	·OH	·H	H_2	O	H_2O_2
Liquid [Yousefi, 2014]	μmol/J	-0.41	0.26	0.26	0.27	0.06	0.04	0.0	0.07
Vapor [Yousefi, 2014]	μmol/J	-0.74	0.0	0.0	0.63	0.74	0.05	0.11	0.0
Liquid	molecules/100 eV	-3.9	2.5	2.5	2.6	0.58	0.4	0.0	0.7
Vapor	molecules/100 eV	-7.1	0.0	0.0	6.1	7.1	0.5	1.1	0.0

Radiolytic Hydrogen Production

Based on the water source evaluation, only the water associated with the fuel rod surface chemisorption, water vapor, and the aluminum rails are potential significant contributors to the H_2 radiolysis production. For water chemisorbed or physisorbed on oxides (i.e., water associated with the aluminum or fuel rod surfaces), the mass of the oxides (rather than just the water content) is used to calculate the absorbed energy for the time period. The radiolytic H_2 production is estimated using a dose rate of 3×10^{15} eV/g/s [Shukla, 2019] and a time period of 12 days, corresponding to the time interval of the third gas sample taken from the cask after sealing. The total dose for the 12-day period (assuming constant dose rate) is $(3.00 \times 10^{15}\ \text{eV/(g·s)})(12\ \text{days}) = 3.11 \times 10^{21}\ \text{eV/g} = 3.11 \times 10^{19}\ 100\ \text{eV/g}$.

Aluminum Components

For aluminum (oxy)hydroxide sources, the total mass of (oxy)hydroxide is calculated based on the estimated exposed aluminum surface area, the assumed (oxy)hydroxide layer thickness, and the density of the (oxy)hydroxide (2.53 g/cm^3 for bayerite and 3.01 g/cm^3 for boehmite [Wefers, 1987]). The absorbed energy (in 100 eV) is calculated by multiplying the (oxy)hydroxide mass by the total dose. To account for limited H_2 sources, the predicted radiolytic H_2 yield over 12 days is either the absorbed energy multiplied by G_{H2} for the (oxy)hydroxide *or* the total H_2 inventory of the (oxy)hydroxide, whichever is smaller.

Assuming 8 μm of bayerite remaining as bayerite after drying, the mass of oxide is about 1750 g, containing 605 g or 33.6 mol H_2O. The predicted yield from bayerite over 12 days with a G_{H2} of 0.02 molecules/100 eV is 0.00180 mol H_2, a small fraction of the total inventory in the bayerite. Dividing by the estimated 386 mol He in the cask yields 4.67 ppmv.

Alternatively, assuming 5.2 μm of boehmite (corresponding to complete drying of 8 μm bayerite), the mass of oxide is about 1340 g, containing 201 g or 11.2 mol H_2O. The predicted yield from boehmite over 12 days with a G_{H2} of 0.05 molecules/100 eV is 0.00347 mol H_2, a small fraction of the total inventory in the boehmite. Dividing by the estimated 386 mol He in the cask yields 8.98 ppmv.

Note that bayerite corresponds to a larger total water inventory that could be released over the long term, but (based on currently available G_{H2} data) is predicted to release it more slowly than boehmite. For either assumption, the predicted yield after 12 days is low.

Details of the cask design are not readily available, and the aluminum surfaces forming the cells and associated with the neutron absorbers are not included in the base aluminum surface calculation. Performing a similar analysis to that for the aluminum rails for the aluminum surfaces in the cell matrix

(assumed not to be exposed) predicts a 12-day yield of 0.00529 mol / 13.7 ppmv H_2 assuming bayerite and 0.0102 mol / 26.3 ppmv H_2 assuming boehmite, i.e., although these surfaces could potentially hold a large inventory of chemisorbed water, the impact on the 12-day radiolytic H_2 would be relatively small.

Fuel Rod and Other Zr Surfaces

For the fuel rod surface water, the same type of calculation applies, except for the handling of the water inventory. The initial surface water on the ZrO_2 is based on three molecular layers of water on the surface (with additional effective surface area due to fissures and crud). The total nominal area of all fuel rods was estimated to be 978 m^2. Adding the 37% surface area for additional Zr components gives a total ZrO_2 surface area of 1340 m^2. Accounting for three monolayers of water at 0.3 mg/m^2/monolayer and multiplying by a factor of three to account for the oxide fissures and crud, the total mass of water is estimated as 3.62 g or 0.201 mol H_2O (0.147 mol on the fuel rods and 0.0543 mol on the additional Zr components). Dividing 0.201 mol H_2 by the 386 mol He estimates the maximum H_2 yield from physisorbed/chemisorbed water on ZrO_2 as 520.3 ppmv. If no exchange of water occurs between the ZrO_2 surface and the water vapor, the surface water on ZrO_2 is essentially fully consumed by radiolysis and the 520.3 ppmv of hydrogen is generated within 12 days due to the application of the G-value of 0.47 molecules/100 eV and the high energy deposition into the oxide layer in that time (3.11×10^{19} 100 eV/g).

For the assumption of replenishment, as this surface water is depleted by radiolysis, it can adsorb additional water from the water vapor in the gas to maintain an equilibrium balance between adsorbed and gas-phase water. A conservative estimate is that the total inventory of free and surface water be used as the limiting inventory for radiolysis from all of these inventories. As a result, the radiolytic yield will first be calculated for the Zr components, water vapor, and steel surfaces and then the sum of these yields will be the H_2 production from the combined free and surface water inventory.

The absorbed energy is calculated for the full oxide mass, assuming an average ZrO_2 thickness of 39 μm on the fuel rods (half that thickness on the other Zr components) and ZrO_2 density of 5.68 g/cm^3. This is a conservative approach, since not all of the energy absorbed by the ZrO_2 oxide will be directly applied to the surface radiolysis.

The estimated ZrO_2 mass is about 257 kg (217 kg for the fuel rods with 39-μm-thick oxide and 40 kg for the additional Zr components with 19.5-μm-thick oxide). The predicted yield based on G_{H2} and the 12-day absorbed dose for the ZrO_2 is 5.26 mol H_2 (equivalent to 13600 ppmv) for the fuel rods and 0.973 mol H_2 (equivalent to 2520 ppmv) for the additional Zr surface.

Water Vapor

An initial 2% (20000 ppmv) water vapor content is used as a preliminary estimate to calculate the impact of water vapor content on the radiolysis. This water content corresponds to an estimated 7.72 mol / 139 g water vapor (based on the estimated moles of gas in the cask). The predicted radiolytic H_2 generation over the 12-day period (water vapor mass multiplied by the dose and G_{H2} for water vapor) is 0.0034 mol H_2, corresponding to 8.7 ppmv.

Steel Surfaces

For the steel surface, the radiolytic yield is calculated using the water G_{H2} of 0.47 molecules/100 eV and the estimated 0.237 g of physisorbed/chemisorbed water initially predicted on the steel surface, which predicts 5.76×10^{-6} mol H_2 (<1 ppmv) over 12 days.

For the case of water replenishment of the fuel surface (with ZrO_2), the total predicted radiolytic yield from free and surface water over 12 days is 6.24 mol H_2, equivalent to 16100 ppmv, which is about 78.5% of the total estimated free and surface water inventory. The total radiolytic H_2 is overwhelmingly dominated by that from the Zr surfaces due to the assumption of energy transfer from the oxide to the adsorbed water.

Summary

The water content, post-dryout, of the HBU Demonstration cask and the radiolysis of those waters causing hydrogen production, were estimated. Potential consumption of hydrogen by gettering by the fuel clad and other zirconium alloys was not estimated. Chemical back reactions were not considered.

A number of assumptions were made in estimating contributions to the free, physisorbed, and chemisorbed waters associated with the fuel rod surface and structural components in the cask, and the hydrogen generation therefrom. This study constructs a component-residual water content set and estimates the total hydrogen and the hydrogen production rate via radiolysis of this set to identify the primary H_2 sources and their relative impacts.

Table 5 shows the calculated values of both potential total inventory and 12-day and 40-year radiolytic generation levels. These values are to be considered relative and qualitative. The specific assumptions and estimates made in the calculations are contained in the body of this report. For the 40-year analysis, the dose rate was assumed to decay exponentially from the initial value with the half-life of Cs-137 (30.05 y); therefore, the 3×10^{15} eV/g/s dose rate used in the calculation was multiplied by $(40\text{ y})^{-1}\int_{0\text{ y}}^{40\text{ y}}\exp\left(-\frac{\ln(2)t}{30.05\text{ y}}\right)dt = 0.653$ to account for the average dose rate over the 40-year span.

Table 5 Hydrogen production due to radiolysis in the HBU Demonstration Cask

H_2 Source	**Total H_2 inventory (ppmv)**	**H_2 production in 12 days (ppmv)**				**H_2 production in 40 years (ppmv)**
		Assuming no H_2O replenishment of surface water (Case 1)		**Assuming rapid H_2O replenishment of surface water from water vapor (Case 2)**		**Assuming H_2O replenishment**
Free/surface water	20554	0.01	(steel)	0.01	(steel)	20554
		520.3	(ZrO_2)	16133	(ZrO_2)	
		8.7	(vapor)	8.7	(vapor)	
Chemisorbed water (bayerite on rails)	86946	4.67		4.67		3711
Total H_2	**107500**	**534**		**16146**		**24265**
Chemisorbed water (bayerite on cell matrix components)	254816	13.7		13.7		10875

The results from the calculations for a 12-day exposure in the HBU Demonstration cask are:

A. The calculated H_2 production from the aluminum rails (assuming bayerite) is 4.67 ppmv.
B. The calculated H_2 production from the water vapor is 8.7 ppmv
C. The calculated H_2 production from the fuel rod surface water is 520 ppmv (for case 1 of no replenishment of the initial ascribed water) and 16100 ppmv (for case 2 of full replenishment of the initial water). This second case significantly exceeds the amount of physisorbed/chemisorbed

water estimated to initially be on the Zr component surfaces. It is assumed that exchange with the water vapor will replenish the surface water until all water vapor and exchangeable surface water is depleted. The high production quantity from the fuel rod is a result of the relatively large ZrO_2 mass to absorb radiation energy. The inclusion of the total oxide mass for dose accumulation is conservative.

D. Radiolysis on the steel surfaces does not contribute significant radiolytic H_2.

E. The inclusion of the cell matrix aluminum surfaces and the absorber surfaces do not significantly impact the short term H_2 but can impact the longer-term generation if included. A more detailed evaluation of the specific cell matrix design is needed to determine what surface areas are appropriate to address. The tri-hydrated oxide (bayerite) with a conservative (large) thickness of 8 μm was assumed for the water source in Table 5.

References

Agayev, T. N., Faradj-zadeh, I. A., Aliyev, A. G., Eyubov, K. T., & Aliyev, S. M. (2017). "Regularities of radiation and heterogeneous processes in contact of Zr and Zr1% Nb alloy with water". Вопросы атомной науки и техники.

Al-Abadleh, H.A and Grassian, V. H.; "FT-IR Study of Water Adsorption on Aluminum Oxide," Langmuir 2003, Vol 19 pages 341 – 347.

Arkhipov, O. P., Verkhovskaya, A. O., Kabakchi, S. A., & Ermakov, A. N. (2007). Development and verification of a mathematical model of the radiolysis of water vapor. Atomic energy, 103(5), 870-874.

ASTM International. "Standard Guide for Drying Behavior of Spent Nuclear Fuel." ASTM C1553–16. West Conshohocken, Pennsylvania: ASTM International. 2016.

Boyd, A. W., and O. A. Miller. "Radiolysis of water vapor with fission fragments." Canadian Journal of Chemistry 46.24 (1968): 3773-3778.

Bryan, Charles, Russell Jarek, Chris Flores, Elliott Leonard: High Burn-up Demonstration Cask: SNL Gas Analyses: Sandia National Laboratories ASTM Nuclear Fuel Drying Workshop January 29, 2019a; also in SNL report Bryan, Charles R., Russell L. Jarek, Chris Flores, Elliott Leonard, Analysis of Gas Samples Taken from the High Burnup Demonstration Cask, Sandia National Laboratories, SANDIA REPORT SAND2019-2281.

Bryan, C.R., S.G. Durbin, E. Lindgren, A.G. Ilgen, T.J. Montoya, T. Dewers, D. Fascitelli. "SNL Contribution: Consequence Analysis for Moisture Remaining in Dry Storage Canisters After Drying," Sandia National Laboratory, SAND2019-8532 R, 2019b.

Byers, W.A.; "Pressurized water reactor core crud mapping," in 18th international conference on nuclear engineering (ICONE 18), Xian China, 2010.

CNWRA. Extended Storage and Transportation: Evaluation of Drying Adequacy. Authors: H. Jung, P. Shukla, T. Ahn, L. Tipton, K. Das, X. He, and D. Basu, San Antonio, Texas: Center for Nuclear Waste Regulatory Analyses. 2013.

Crumière, F., Vandenborre, J., Essehli, R., Blain, G., Barbet, J., & Fattahi, M. (2013). LET effects on the hydrogen production induced by the radiolysis of pure water. Radiation Physics and Chemistry, 82, 74-79.

d'Entremont, A.L. R.L. Kesterson, and R.L. Sindelar, "Evaluation of Hydrogen Generation in High Burnup Demonstration Dry Storage Cask," SRNL-STI-2020-00268, August 2020a.

d'Entremont, A. L., Fuentes, R. E., Shalloo, M. G., Knight, T. W., Sindelar, R. L., Thermal Dehydration of Aluminum (Oxy)hydroxides on Fuel Cladding Material, Proceedings of Waste Management Symposia 2020, #20200, 2020b.

Dylla, H.F.; "The Problem of Water in Vacuum Systems", presentation at CERN Accelerator School May 2006

Elliot, A. J., and D. M. Bartels." The reaction set, rate constants and g-values for the simulation of the radiolysis of light water over the range 20° to 350°C based on information available in 2008". No. AECL—153-127160-450-001. Atomic Energy of Canada Limited, 2009.

Elliot, A.J., Bartel, D. M., AECL Report-11073, Chalk River, Canada, 2009

Fort, James A., D.J. Richmond, J.M. Cuta, S.R. Suffield, "Thermal Modeling of the TN-32B Cask for the High Burnup Spent Fuel Data Project", July 30, 2019,PNNL-28915

Hazelton, R.F.;"Characteristics of Fuel Crud and its Impact on Storage, Handling, and Shipment of Spent Fuel" - September 1987 Prepared for the U.S. Department of Energy under Contract DE-AC06-76RLO 1830 Pacific Northwest Laboratory Richland, Washington 99352 PNL--6273 DE88 000914

Garibov, A.A., T.N. Agayev, G.T. Imanova, K.T. Eyubov, "Kinetics of radiation and catalytic decomposition of water in the presence of nano-zirconium dioxide." issn 1562-6016. PAST. 2015. №5(99), p. 48.

Hering, G., "Spent Nuclear Fuel Storage Demo Heats Up: Ten-Year Demonstration to Begin in 2017", EPRI Journal, 2016, 26–28.

Holmes, H. F., Fuller Jr, E. L., & Beh, R. A. (1974). "Adsorption of argon, nitrogen, and water vapor on zirconium oxide". Journal of Colloid and Interface Science, 47(2), 365-371.

Hou, B., Kim, S., Kim, T., Kim, J., Hong, S., Bahn, C. B., ... & Kim, J. H. "The hydration structure at yttria-stabilized cubic zirconia (110)-water interface with sub-Ångström resolution". *Scientific reports*, *6*, 27916. (2016).

Jenson, B., "TN 32 Dimensions For Thermal Analysis", Drawing of TN-32 cask provided courtesy of K. Waldrop, EPRI.

Kabakchi, S.A.,O.P. Arkhipov, M.L. Lukashenko: " Specific Features of the Radiolysis of Water and Aqueous Solutions of H2 and O2 by Mixed n,γ-Radiation with a High Portion of the Neutron Component.", High Energy Chemistry 47, 2013, 147-151.

Kaddissy, J.; "Hydrogen production from irradiated aluminum hydroxide and oxyhydroxide". PhD thesis. Material chemistry. Université Paris-Saclay, 2016.

Knoll, R.W., et al., "Evaluation of Cover Gas Impurities and Their Effects on the Dry Storage of LWR Spent Fuel," PNL-6365, DE88 003983, PNNL, November 1987.

Knott, R. P., Kesterson, R. L., Hallstadius, L. G., & Young, M. Y. (2003, March). "Advanced PWR fuel designs for high duty operation". In Proceedings from the ENS TopFuel 2003 Meeting (pp. 16-19).

Köck, E. M., Kogler, M., Klötzer, B., Noisternig, M. F., & Penner, S. (2016)." Structural and electrochemical properties of physisorbed and chemisorbed water layers on the ceramic oxides Y2O3, YSZ, and ZrO2". ACS applied materials & interfaces, 8(25), 16428-16443

LaVerne, J.A.,L. Tandon,; "H2 Production in the Radiolysis of Water on UO2 and Other Oxides". J. Phys. Chem. B 107, 2003, 13623-13628.

Le Caër, S.; " Water Radiolysis: Influence of Oxide Surfaces on H2 Production under Ionizing Radiation", Water 3, 2011, 235-253.

Pastina. B. and LaVerne,J. A. "Effect of Molecular Hydrogen on Hydrogen Peroxide in Water Radiolysis", J. Phys. Chem. A 2001, 105, 9316-9322.

Petrik, N. G., Alexandrov, A. B., & Vall, A. I. (2001).” Interfacial energy transfer during gamma radiolysis of water on the surface of ZrO2 and some other oxides”. The Journal of Physical Chemistry B, 105(25), 5935-5944.

Poloski, A., Hanson, B. " Initial Concepts for a Small Scale Drying Study" ASTM Subcommittee C26.13 Meeting – Spent Fuel and High Level Waste January 28, 2019

Shukla, P, R.L. Sindelar, P.-S. Lam, “Consequence Analysis of Residual Water in a Storage Canister – Preliminary Report,” SRNL–STI–2019–00495

Sindelar, R.L., M.J. Connolly, J.J. Jarrell, D.T. Herman, and W.H. Bates, *Technology Development for Dry Storage of Aluminum-Clad Spent Nuclear Fuel*, Paper 20490 at WM2020, March 2020.

Skotnicki, K., & Bobrowski, K.; “Molecular hydrogen formation during water radiolysis in the presence of zirconium dioxide.” Journal of Radioanalytical and Nuclear Chemistry, 304(2), 473-480. (2015)

Spinks,J. W., Woods, R.J.; "An Introduction to Radiation Chemistry", 3rd ed., Wiley Interscience, New York, 1990.

Waldrop,K. “RE: [EXTERNAL] cask design.” Received by Robert Sindelar, 08 July, 2020.

Wang, M.; " Irradiated Assisted Corrosion of Stainless Steel in Light Water Reactors" – Focus on Radiolysis and Corrosion Damage. hal-00841142, 2013

Wefers,K. and Misra,C.; "Oxides and hydroxides of aluminum," Alcoa Laboratories Pittsburgh, PA Alcoa Technical Paper #19, 1987.

Wertsching, A. K. "Material Interactions on Canister Integrity during Storage and Transport." DOE/SNF/REP-104 (2007)

Westbrook,M.L. R.L. Sindelar, D.L. Fisher, "Radiolytic hydrogen generation from aluminum oxyhydroxide solids: theory and experiment." J. Radioanalytic and Nuclear. Chem. 303, 2015, 81-86.

Wittman, R.S.; "Radiolysis Model Sensitivity Analysis for a Used Fuel Storage Canister", FCRD-UFD-2013-000357, PNNL-22773, 2013.

Wilson, W., and R. J. Comstock. Potential impacts of crud deposits on fuel rod behavior on high powered PWR fuel rods. No. IAEA-TECDOC--1128. 1999.

Yousefi, N. "Gamma-Radiolysis Kinetics of Liquid, Vapour and Supercritical Water.", Master’s thesis, University of Western Ontario, 2014.